RSC Advances

ROYAL SOCIETY OF CHEMISTRY

www.rsc.org/advances

Cite this: DOI: 10.1039/c0xx00000x

www.rsc.org/materials

Paper

A Mechanistic Study on Amphiphilic Block Co-polymer Poly(butadiene-*b*-(ethylene oxide)) Vesicles Reveals Water Permeation Mechanism through Polymeric Bilayer

Fang He[a] and Yen Wah Tong*[b,c]

Received (in XXX, XXX) Xth XXXXXXXXX 20XX, Accepted Xth XXXXXXXXX 20XX
DOI: 10.1039/b000000x

The objective of this work is to study the interdependence between the membrane tension and osmotic permeability of di-block copolymer PBD-PEO (poly(butadiene-*b*-(ethylene oxide))) bilayer. Experiments were conducted to decouple the contribution of membrane tension into (1) PEO conformation; (2) area stretching modulus (κ_a); (3) bending rigidity modulus (κ_c); (4) chemical crosslinking on PBD segment. A range of different PBD-PEO block copolymer formulation has been included with similar hydrophilic/lipophilic balance (HLB) factor and end-group for a systematic comparative study. We have also demonstrated the applicability of a membrane probe, laurdan, to study small-to-medium molecular weight PBD-PEO polymersomes and the results are consistent with area stretching and bending rigidity moduli measured otherwise. In addition, we are able to correlate the membrane rigidity with the osmotic permeability, to fortify our conclusion that the solute permeation mechanism through block copolymer bilayer is dominated by (1) mass transfer at the interfacial region, and (2) diffusion through the hydrophobic segment. By subjecting the block polymer to a chemical crosslinking in the PBD segment, the polymer was engineered to be much more rigid and much less permeable to osmotic flux.

1. Introduction

Amphiphilic block copolymers have many applications due to their versatility, ranging from medicine to material science, for instance the construction of nano-reactors, drug delivery systems, nanoporous membranes and biosensors.[1-10] Bearing resemblance to natural amphiphilic lipids, synthetic amphiphilic block copolymers comprising of covalently bonded hydrophobic and hydrophilic segments, possess intrinsic ability to self-assemble into several mesophases. By adjusting the block length and hydrophilic/lipophilic balance (HLB) factor, multiple morphologies and architectural varieties of block copolymer aggregates can be synthesized, ranging from micelles, rods, tubules to vesicles. More specifically, morphologies of the self-assembled block copolymers can be modified by the degree of polymerization, the Flory-Huggins interaction parameter χ and the hydrophilic volume fraction f.[11-14] Poly(butadiene-*b*-(ethylene oxide)) (PBD-PEO) amphiphilic block copolymers are of particular importance in studying lyotropic phase behavior due to the low glass transition temperature of the polybutadiene (PBD) block of about -10^{o}C which renders the block copolymers dispersible in aqueous environment.[15] The hydrophilic segment of poly(ethylene oxide) (PEO), also known as poly(ethylene glycol) (PEG), imparts good biocompatibility to the copolymer.[16] These two factors make PBD-PEO block copolymer vesicles widely suitable for various applications and in particular, due to remarkable stability, it is often used in substitution of lipid bilayers in synthetic amphiphilic bilayer for reconstituting integral membrane proteins. Examples of membrane proteins incorporated into the polymer bilayers include the mechano-sensitive channel protein MscL,[17] the pore-spanning OmpF,[18] and the water channel protein aquaporins.[19] However prior to protein reconstitution into the amphiphilic polymeric bilayer, it is imperative to understand this polymeric system thoroughly, especially in the context of mechanical stiffness and membrane tension since these mechanistic factors are widely acknowledged to impact and modulate protein functionality.[20]

Though there are various methodologies available for measuring membrane tension, for instance Langmuir-Blodgett trough (LB trough), it is only applicable to the simple flat bilayer measurement. In addition, it is time consuming and lacks versatility, and thus unsuitable when there are more membrane additives in the bilayer for instance cholesterol or membrane proteins. In this paper, we intend to demonstrate the usage of the membrane probe laurdan to quantify membrane tension in the polymer bilayer. By incorporating laurdan into the polymersomes, we can examine the *in situ* membrane tension in a 3-dimensional setting to include the contributions of angular tension. Laurdan, or 6-dodecanoyl-2-dimethylamino naphthalene (MW = 353.55 g/mol) is an extrinsic fluorescent membrane probe which exhibits sensitivity to polarity and molecular dynamics of dipoles in its microenvironment. Being insoluble in aqueous solvents, it can be incorporated into the amphiphilic bilayer for detection of membrane rigidity. When integrating into the membrane, the lauric acid chain provides strong hydrophobic anchorage into the hydrophobic segment, leaving its fluorescent

moiety at the hydrophobic/hydrophilic interface. It has been hypothesized that the emission spectral shift in the extrinsic dye laurdan is due to reorientation of the water molecules at the hydrophilic/hydrophobic interface and thus showing the changes in the extent of local coupling to the solvent dipoles.[21] When there is high water content at the interface as when the membrane is in *liquid-crystalline* phase, the emission peak of laurdan is at 490 nm; conversely when there is little water content at the interface as when the membrane is in *gel* phase, the emission peak of laurdan is at 440 nm.[22] Here, we hypothesize that the energy loss due to re-alignment of water molecules would be proportional to the chain rigidity, reflecting both the angular and lateral perspectives.

Discher and co-workers have previously conducted mechanistic studies on block copolymer of molecular weight greater than 3kDa and of hydrophobic thickness, *d*, more than 8 nm.[23-27] In this work, we have focused on low-to-medium molecular weight block copolymers and presented different methodologies to examine the membrane tension implicitly. With the increasing molecular weights and block lengths, polymeric chains exhibit more flexibility but beyond a certain threshold value of the hydrophobic segment molecular weight, the inter-digitation between the upper and lower leaflets leads to a greater extent of chain entanglement and thus retards the lateral diffusivity.[27, 28]

The overall aim of this paper is to systematically study the mechanistic effects of the diblock copolymer PBD-PEO in modulating PEO chain packing, and rigidity of the polymeric chains. Based on the mechanistic study, we hypothesize that the water permeation mechanism through the block copolymer bilayer is such that with increasing chain rigidity, water permeation rate (P_h) through the polymeric bilayer would be retarded in accordance to the bending rigidity modulus (κ_c) of the polymeric bilayer. This is due to the rate-limiting step of solutes permeating across the interfacial region and diffusing through the thick hydrophobic core by creating a cavity into the bilayer.

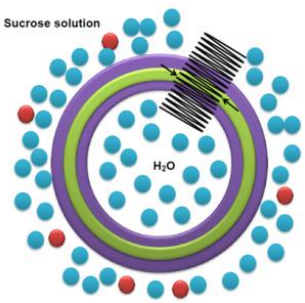

Fig 1. The schematic of the osmotic flux through the amphiphilic bilayer influenced by the bilayer tension.

2. Experimental Section

2.1 Materials

PBD-PEO block copolymers were purchased from Polymer Source (Canada). The mini-extrusion set and polycarbonate (PC) membranes were purchased from Avanti Polar Lipids, Inc. 6-dodecanoyl-2-dimethylaminonaphthalene (laurdan), were purchased from Molecular Probes, Invitrogen. Sodium sulfite and ammonium persulfate were purchased from Sigma Aldrich (Singapore). Chloroform (ACS grade), ethanol (HPLC grade) were purchased from Merck (Singapore).

2.2 Synthesis of polymersomes

Vesicle formation. PBD-PEO polymersomes were fabricated using the film rehydration method. Briefly, PBD-PEO polymer was firstly dissolved in chloroform, which was then slowly removed by evaporation overnight. A suitable solvent (DI water or 1x PBS) was then added to the dry film. After stirring for 6 h at 300 rpm at 45°C, polymersomes were fabricated. All polymersome solutions were subjected to extrusion through a PC membrane for at least 21 times to reduce the size of polymersomes to unilamellar vesicles, unless stated otherwise. The sizes of the polymersomes were verified with Dynamic Light Scattering ZetaSizer (Malvern Instruments Ltd, USA) and Transmission Electron Microscopy (JEOL JEM-2100F, JOEL Japan).

Crosslink polymersomes. Extruded PBD-PEO polymersomes were crosslinked via a two-step free radical crosslinking. Firstly ammonium persulfate was added to vesicle solution in 1:1 molar ratio, and the mixture was sealed in nitrogen gas protection. Crosslinking was initiated by injection of sodium sulfite solution into the mixture and reaction ran at 40°C for 1 h. Excess initiators were removed by dialysis.

2.3 Area stretching modulus and bending rigidity

Langmuir-Blodgett trough was custom-made by NIMA (KSV NIMA, UK) (45 cm × 10 cm) from a single piece of pure PTFE with two independently controlled Delrin barriers for symmetric monolayer compression. Subphase area 450 cm^2 (45 × 10 cm), monolayer containment area 415 cm^2, subphase volume 225 mL. The block copolymers were dissolved in chloroform at 1 mg/ml. Before each run, the trough was thoroughly cleaned by chloroform followed by excess ultrapure (UP) water. After filling the trough with UP water, 50 µL of 1 mg/mL polymer in chloroform solution was slowly injected to the trough and sufficient time was allowed for it to spread and stabilize. The monolayer was then compressed and expanded slowly at 20 cm^2/min to avoid the dynamic effect.

One method to study the polymer packing is by examining the compressibility modulus of the monolayer, which can be calculated according to Equation (1):

$$\varepsilon = -A\left(\frac{\delta\pi}{\delta A}\right) \quad (1)$$

where ε is the compressibility modulus(pN/nm), A is the area of the monolayer (nm^2/molecule), π is the surface tension in the LB trough (pN/nm). It has been shown by Israelachvili that the monolayer compression rigidity ε_{mon} is determined by the surface energy of the amphiphile/water interface γ,[29] and the area stretching modulus κ_a is twice that of the monolayer ε_{mon}, alternatively expressed as following:

$$\kappa_a = 4 \times \gamma \quad (2)$$

The bilayer bending rigidity can be calculated as

$$\kappa_c = \kappa_a \times \beta \times d^2 \quad (3)$$

where d is the thickness of hydrophobic segment, and β is the coupling factor.[30] β assumes a value of 1/48 for bilayer that is free to slide over one another and a value of 1/12 for completely coupled and rigid bilayer. The hydrophobic thickness of PBD-PEO bilayer referenced is shown in Table 1.

Table 1 The thicknesses of hydrophobic segments of different PBD-PEO-OH polymers

Sample	Formula	d^a (nm)
PBD22-PEO14-OH	PBD_{22}-PEO_{14}	8.4
PBD33-PEO22-OH	PBD_{33}-PEO_{20}	9.0
PBD46-PEO30-OH	PBD_{46}-PEO_{30}	9.8

[a] Hydrophobic thickness of the bilayer measured from simulation[30]

2.4 Membrane rigidity and thermal expansivity

Laurdan was added at 0.6 wt% to extruded polymersomes solution and laurdan/polymer mixtures were incubated for 3 h at room temperature (25°C). Multiple excitation and emission readings were recorded using microplate reader (Tecan Infinite 200 PRO, Zurich, Switzerland) at controlled temperature settings to probe for maximal excitation and emission wavelengths. A commonly used parameter GP (Generalized Polarization) value was calculated to reflect the chain rigidity of the lipid bilayer,[31] since the emission peak at 490 nm is associated with *liquid-crystalline* phase, and 440 nm is associated with *gel* phase.

$$GP = \frac{I_{440} - I_{490}}{I_{440} + I_{490}} \quad (4)$$

When there is absence of characteristic emission peaks at 440nm and 490nm, the energy dissipation term from laurdan from the excited state can be used to represent the shift in emission energy. It is calculated according to the following Equation (5):

$$\Delta q = \frac{1}{\lambda_{ex}} - \frac{1}{\lambda_{em}} \quad (5)$$

where Δq is the difference in the wavenumber (cm^{-1}), λ_{ex} and λ_{em} are the peak excitation wavelength and peak emission wavelength of laurdan respectively.

The thermal transition of the amphiphilic bilayer can be studied via laurdan at the controlled temperature settings (*e.g.*, 25°C, 30°C, 35°C, 40°C). The solvent local polarity Δf has been found empirically correlated with energy dissipation Δq (cm^{-1}) in linear relationship:[21]

$$\Delta f = c_0 + c_1 \Delta q \quad (6)$$

where c_0 = -0.19 and c_1 = 6.9 ×10^{-5} cm. A graph of Δf versus T can be plotted explicitly to illustrate the thermal transition of the amphiphilic bilayer. In the liquid-crystalline phase or the polymer membrane, the polarity Δf increases weakly with increasing temperature T; however at the thermal transition temperature of the lipid bilayer, the solvent polarity increases sharply. The thermal polarizibility is defined as $\delta(\Delta f)/\delta T$.

2.5 Osmotic permeability

The osmotic permeability of the polymersome solution was investigated using stopped-flow spectroscopy (Applied Photophysics Ltd, UK)[32] The polymersome solution was rapidly mixed with 300 mOsm sucrose solution in a 1:1 volume ratio. The kinetics of polymersomes shrinking was recorded and light scattering data was fitted into single an exponential function. The following formula was applied to evaluate the osmotic permeability of polymersomes (i.e. water flux per unit of polymersome membrane area per unit time).

$$P_h = \frac{k}{(S/V_0) \times V_w \times \Delta_{OSM}} \quad (7)$$

where k is the dimensionless exponential factor in initial rise in the exponential function; S is the initial surface area of the polymersomes (nm^2); V_0 is the initial volume of the polymersomes (nm^3); V_w is the molar volume of water (18 cm^3/mol); Δ_{OSM} is the osmolarity difference across the polymersome bilayer driving the shrinkage of the polymersomes (150mOsm), P_h is the osmotic water permeability coefficient (μm/sec).

2.6 Imaging

Sample preparation for TEM. The samples for imaging of nanoparticles were prepared by dropping a suspension of the sample on the TEM copper grids and vacuum dried. The grids were thoroughly dried in air overnight prior to TEM imaging.

2.7 Statistical analysis

All the membrane rigidity study with laurdan and microplate reader was conducted with at least 5 independent test samples (N = 5). Mean, standard deviation (S.D.), error calculations, student's t-tests (unpaired sample) were performed using Microsoft Excel Data analysis package (2010) for statistical analysis. The stopped-flow data was evaluated with at least 20 independent test samples for each vesicle or protein concentration (N = 20). The data fitting into the single exponential function to evaluate osmotic permeability was performed using OriginPro 8.1 (OriginLab, Northampton, MA).

3. Results and Discussion

3.1 Morphology of PBD-PEO polymersomes

The exact formulation of PBD-PEO polymers is tabulated below, indicating the polymer structure, molecular weight, end group, hydrophilicity/lipophilicity balance (HLB) factor, and hydrophilic volume ratio (f value). The f value would determine the architectural variety formed by the diblock copolymers; with the f value between 0.25 and 0.45, these polymers are capable of forming vesicles, instead of micelles or inverted structures.[23]

Table 2. A list of diblock PBD-PEO polymers used to synthesize polymersomes. Mw is the molecular weight, HLB factor is hydrophilicity/lipophilicity balance (calculated as $20Mw_{PEO}/Mw$), and *f* value is hydrophilic volume fraction (assuming that ρ_{PEO} = 1.13g/cm^3, ρ_{PBD} = 1.06g/cm^3).[33]

Sample	Addition[a]	MW[b]	Formula	End Group	HLB[c]	*f*[d]
PBD22-PEO14-OH	(1,2)	1800	PBD_{22}-PEO_{14}	OH	6.67	0.319
PBD22-PEO14-NH_2	(1,2)	1800	PBD_{22}-PEO_{14}	NH_2	6.67	0.319
PBD33-PEO14-OH	(1,2)	2400	PBD_{33}-PEO_{14}	OH	5.00	0.238
PBD33-PEO20-OH	(1,2)	2700	PBD_{33}-PEO_{20}	OH	6.67	0.319
PBD33-PEO20-NH_2	(1,2)	2700	PBD_{33}-PEO_{20}	NH_2	6.67	0.319
PBD46-PEO30-OH	(1,2)	3800	PBD_{46}-PEO_{30}	OH	6.84	0.327
PBD46-PEO30-NH_2	(1,2)	3800	PBD_{46}-PEO_{30}	NH_2	6.84	0.327
PBD93-PEO52-OH	(1,4)	7300	PBD_{93}-PEO_{52}	OH	6.30	0.301

[a] (1,2) addition indicates the C=C is on the side chain and (1,4) addition indicates that C=C is on the backbone of PBD segment (SI Fig 6). [b] MW, molecular weight (g/mol). [c] HLB, hydrophilicity/lipophilicity balance factor measures the relative ratio between PBD and PEO blocks. [d] f value, the hydrophilic volume fraction measures the relative volume ratio between PBD and PEO blocks, and it determines the architectural variety formed by the block copolymer.

Without subjecting the polymersomes to extrusion, the size of the polymersomes is in the micron range in diameter, with high polydispersity and multiple lamellae structure as seen from DLS (Dynamic Light Scattering) (data not shown) and CLSM (Fig 2). This might be attributed to the ionic interaction in the hydrophilic PEO segment.[34, 35] Polymersomes were extruded through polycarbonate (PC) membranes with track-etched pore size of 100nm. After the mini-extrusion, the size of polymersomes was measured via DLS and TEM, and found to be around 160 nm (Fig 2).

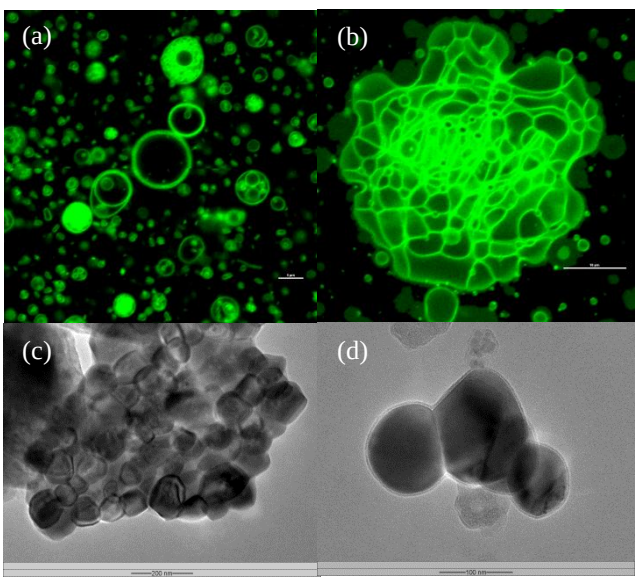

Fig 2. CLSM and TEM images of polymersomes (1 mg/ml PBD33-PEO20-OH) vesicles. (a) Without extrusion, the uncrosslinked polymersomes are polydispersed in the size range of 10 μm with multi-lamellae structure (polymersomes were labelled by Coumarin-6), scale bar = 5μm; (b) the close-up shows the extensive network formed inside the giant vesicle, scale bar = 10μm; (c) after extrusion through 100 nm pore size polycarbonate (PC) membrane, the size of the crosslinked polymersomes is 160 nm, scale bar = 100nm; (d) the close-up of three distinctive polymersomes, scale bar = 200nm. The mini-extrusion setup and procedures haave been illustrated in SI Fig 5.

3.2 Molecular weight dependent PEO chain packing in monolayer

One way to understand membrane tension is by examining the PEO chain packing in the polymeric monolayer through LB trough experiment. The transition in PEO chain packing conformation from low surface tension (π < 10m N/m) to high surface tension (π > 20 mN/m) can be defined by the intersection point between the lines at these two regimes (Fig 3). There exists a fairly linear relationship (*R*-square = 0.987) between the molecular weight of the polymer and the transition from a flat-like state to a brush-like state; this is only applicable to polymers with the same composition of the end group and HLB factor of the polymer (Fig 3). The additional data of PBD33-PEO14-OH and PBD46-PEO30-NH_2 monolayers have been included to observe for any difference in effect induced by altering the HLB factor or end groups.

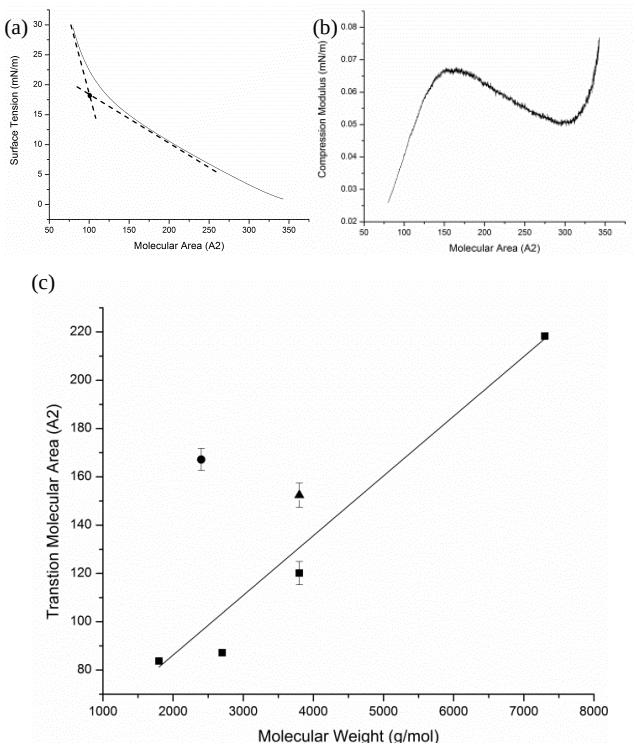

Fig 3. (a) The transition from low surface tension (π<10mN/m) to high surface tension (π>20mN/m) is defined by the intersection point between two lines fitted to the two regimes; (b) the corresponding compressibility modulus of the monolayer; (c) graph of the transitional molecular area (A^2) versus molecular weight of the block copolymer. Adjusted *R*-square has been calculated with exclusion of PBD33-PEO14-OH, PBD46-PEO30-NH_2, PBD93-PEO52-OH since they differ from the rest by their HLB factor or end group or the position of C=C in PBD segment. PBD-PEO samples are represented according to their different chemical

structures: PBD22-PEO14-OH (■); PBD33-PEO14-OH (●); PBD33-PEO20-OH (■);PBD33-PEO20-NH_2 (▲); PBD46-PEO30-OH (■); PBD93-PEO52-OH (■).

As anticipated, with the increasing hydrophobic segment or the decreasing hydrophilic segment alone results in an increase in the surface tension. PBD33-PEO14-OH has been included in the study because this polymer presents a very low HLB factor and hydrophilic volume fraction; this is due to the presence of oddly long hydrophobic PBD segment in this polymer. A delicate and standardized HLB balance is required to maintain the integrity of the diblock polymer structure, as the structure is susceptible to different extent of hydrophobic and/or hydrophilic interaction with the neighbouring polymer molecules or solvent molecules. Alternatively, a substitution in end group from OH to a positively charged group NH_3^+ alters the surface tension of the monolayer, presumably because there is increased interaction between monolayer and water in the subphase. Interestingly, even though the PBD93-PEO52-OH with a *1,4-addition* chemical structure in the hydrophobic segment, distinctive from *1,2-addition* PBD-PEO-OH polymers, molecular packing at the monolayer level is nevertheless proportional to its molecular weight, being insensitive to the chemical structure of the block copolymer. Thus this packing factor represents more of a transition in the PEO chain conformation in the monolayer. However to understand the polymer bilayer completely, the contribution by the PBD segment should be included as well, in particular as water permeation through the hydrophobic segment is hypothesized to be one of the rate limiting steps.

3.3 Area stretching and bending rigidity moduli

In addition to PEO chain packing, lateral packing in terms of the compressibility modulus could be studied via Langmuir Blodgett trough.[33] The surface tension and the compressibility modulus can be controlled by adjusting the fractional trough area available to the polymer monolayer in the LB trough, and the monolayer packing is optimal when compressibility modulus is at its maxima. It is generally assumed that at the maximal compressibility modulus, monolayer packing is optimal and resembles that in self-assembled polymersome structures. The surface energy at the PBD-PEO polymer/water interface is found to be in the range of 32-38 pN/nm, which is in good quantitative agreement with PEE-PEO (poly(ethyl ethylene-*b*-ethylene oxide)) polymer, the fully saturated model of PBD-PEO. β assumes a value of 1/48 for bilayer that is free to slide over one another, and a value of 1/12 for completely coupled and rigid bilayer. In order to make qualitative comparisons between the results obtained from the LB trough and membrane probe studies, β is assumed to be 1/48 here. A strong linearity between the bending rigidity and molecular weight of the polymer has been observed, *i.e.* with the increasing molecular weight, the area stretching modulus and bending rigidity modulus increase proportionally (Fig 4a), and this serves as the basis for comparison with results obtained from the membrane probe laurdan.

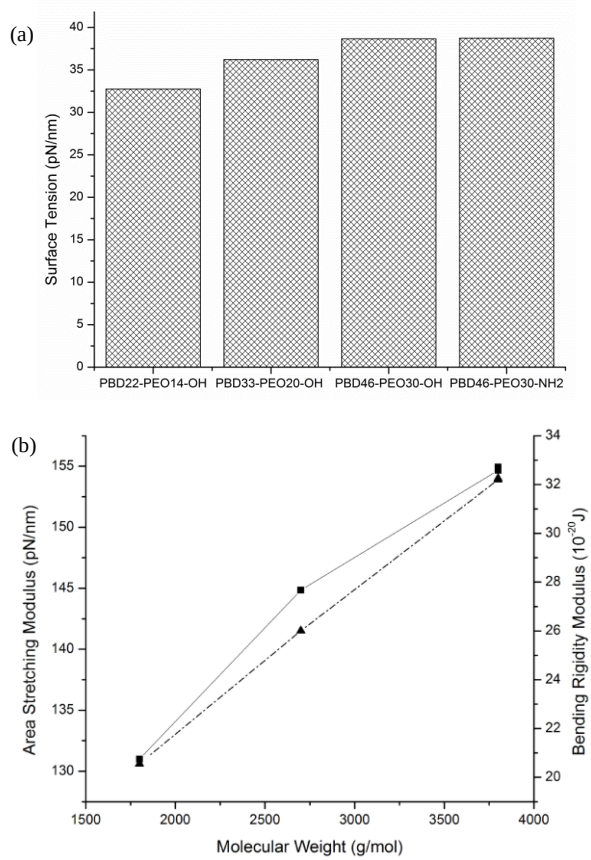

Fig 4. (a) The surface energy of amphiphile/water interface γ (pN/nm) versus molecular weight (g/mol); (b)the area stretching modulus (κ_a/pNnm^{-1}) (■) and bending rigidity modulus (κ_c/pN·nm) (▲) versus molecular weight of the block copolymer (g/mol). In order to make qualitative comparison between the results obtained from LB trough and membrane probe laurdan, β is assumed to be 1/48 in the calculation.

Notably the elastic bending property of the polymer bilayer exhibits some significant increase from that of the pure lipid bilayer (DMPC, DOPC),[36, 37] and more closely resembles to that of cholesterol-lipid hybrid vesicles (**Table 3**). The increase in the bending rigidity modulus indicates that polymersomes are less likely to be influenced by the thermal energy, and thus less susceptible to shape fluctuations, compared to the liposomes.[38] It assists in explaining the polymersomes' apparent superior mechanical stability, shape-retaining ability compared to the natural amphiphilic liposomes.

Table 3. The bending rigidity of different PBD-PEO-OH polymers

Sample	κ_c ($\times 10^{-20}$J)	Experimental condition
DMPC	11.5 ± 1.5	Flickering[37]
DMPC + 20% cholesterol	21.0 ± 2.5	
DMPC + 30% cholesterol	40.0 ± 8.0	
SOPC	9.0 ± 0.6	Entropic tension, electric field[39]
DLPC	3.4 ± 0.7	
POPC	2.5 ± 0.5	
PBD22-PEO14-OH	20.6 ± 2.1[a]	Langmuir Blodgett Trough
PBD33-PEO20-OH	26.6 ± 2.7[a]	
PBD46-PEO30-OH	32.2 ± 3.2[a]	

[a] Values represent the mean ± standard deviation (error bars) with $N = 5$

3.4 Membrane rigidity

Unfortunately LB trough measurements describe the membrane tension at a 2-D lateral perspective, and thus are unable to provide quantitative information about the *in situ* membrane tension in the polymersomes. Thus, it is our intention here to demonstrate the novel application of the membrane probe laurdan to small-and-medium molecular weight block copolymers, these results would be compared and verified with the results compared to the bending rigidity modulus obtained from LB trough.

Laurdan has been previously incorporated laurdan in the lipid bilayer membrane to detect the 3D mechanical strain in the liposome membrane of different sizes.[22] Laurdan indicates the chain rigidity of the bilayer according to the amount of water content present at the hydrophobic/hydrophilic interface. Laurdan has a characteristic emission peak at 490 nm when it is incorporated into the *liquid-crystalline* phase, and 440nm when it is in the *gel*-phase. A commonly used parameter, GP (Generalized Polarization) (Equation 4) value can be calculated to reflect the chain rigidity of the lipid bilayer.[31] However, it is noteworthy that the position of the characteristic emission peaks at 440 nm and 490 nm remain the same in different DOPC/DSPC mixtures (SI Fig 2). In contrast, when laurdan has been incorporated into the block copolymer bilayers, there is no characteristic emission peaks at 440 nm and 490 nm as observed for lipid bilayers, but instead the maximum emission peak shifts according to the rigidity of the polymeric bilayer. Energy dissipation of laurdan from the excited state is then used as a measure of chain rigidity in the polymeric bilayer, and it can be calculated based on Δq, from maximal excitation (λ_{ex}) to maximal emission (λ_{em}) wavelengths as Equation (5).

PBD22-PEO14-OH, PBD33-PEO20-OH and PBD46-PEO30-OH are three block copolymers with very similar HLB factor, hydrophilic volume fraction (*f* value) and chemical structure (Table 2). As the molecular weight increases, it has been found that the membrane rigidity increases proportionally as indicated by the decreasing Δq, which is consistent with results obtained from bending rigidity modulus κ_c. As laurdan is relatively small compared to the size of block copolymer, it would be difficult for laurdan to penetrate into the core of the hydrophobic segment, with a penetration depth of merely 0.4nm below the interface. Therefore the fluorescence readings from laurdan incorporated bilayer do not indicate the coupling between the monolayers. The advantages of this method is that the study is less time-consuming, and reflects the *in situ* membrane rigidity in the setting of polymersomes to better advance our understanding in the bilayer tension, as compared to using the LB trough. This would be easily extended to more complex system for instance the proteo-polymersomes when the use of the LB trough would be very challenging.

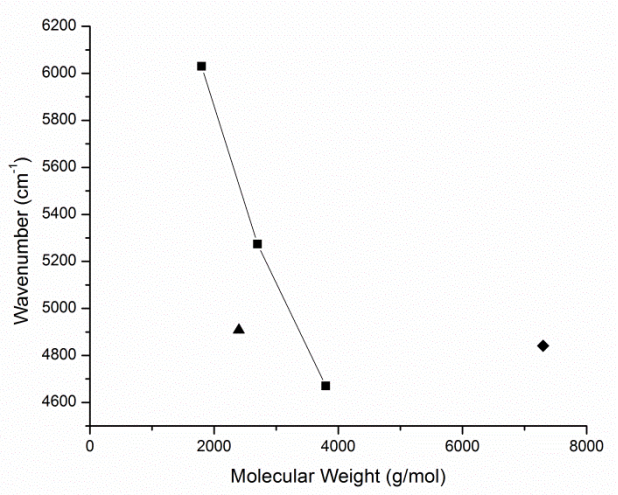

Fig 5. The correlation between energy dissipation in Laurdan fluorescence in term of Δq (cm^{-1}) versus *MW* (g/mol) of the PBD-PEO-OH block copolymer (diameter of the vesicles = 160 nm). The energy dissipation term was represented using Δq, obtained from $\Delta q = q_{ex} - q_{em}$. PBD33-PEO14-OH and PBD93-PEO52-OH are excluded from linearity analysis owing to their difference in HLB factor, and the position of C=C in PBD segment. Various PBD-PEO samples are represented according to their different chemical structures: PBD22-PEO14-OH (■); PBD33-PEO14-OH (▲); PBD33-PEO20-OH (■); PBD46-PEO30-OH (■); PBD93-PEO52-OH (♦).

3.5 Thermal transition and expansivity

The thermal expansivity of the polymeric bilayer can also be studied via the laurdan probe under controlled temperature settings. Even though temperature has increased from 25°C to 40°C, the absence of a sharp increase in the solvent polarity (Fig 6) is consistent with the fact that block copolymers do not exhibit a clear, distinctive transition temperature like lipids. The local polarity of laurden in the *gel*-phase lipid bilayer has a value of 0.15 and that of the *liquid-crystalline*-phase lipid bilayer is 0.3.[21] In a stark contrast to lipid bilayer, the resulting solvent polarity of PBD-PEO polymers ranging only from 0.16 to 0.24 confirms that these block copolymer bilayers are more of rigid *gel* phase characteristics than liquid-*crystalline* phase behaviour.

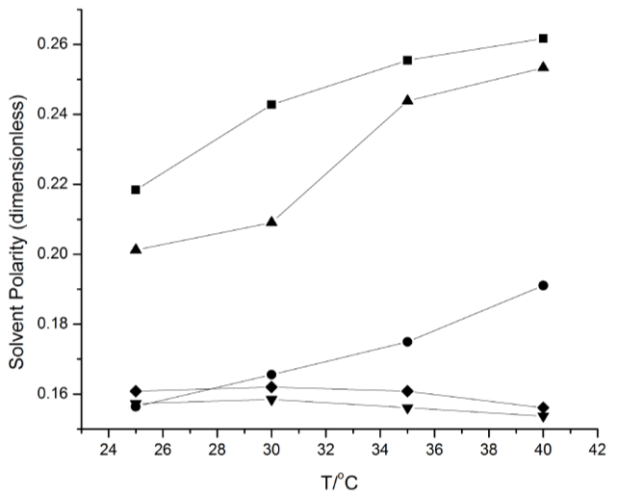

Fig 6. Thermal expansion curve of various PBD-PEO-OH membranes from 25°C to 40°C as a function of temperature for various PBD-PEO samples: PBD22-PEO14-OH (■); PBD33-PEO14-OH (●); PBD33-

PEO20-OH (▲); PBD46-PEO30-OH (▼); PBD93-PEO52-OH (♦). The slope of the curve d(Δf)/dT is defined as thermal polarizability. Different from lipids, PBD-PEO-OH block copolymers do not have distinctive phase transition temperature, which is indicated by the lack of a sharp increase in the curve.

3.6 Osmotic permeability and mechanism of water permeation

The osmotic permeabilities of the polymersomes in DI water and 1x PBS were evaluated by stopped-flow spectroscopy and calculated according to the exponential factor in the initial rise (up to 5 seconds) of the light scattering data. Single exponential curve fits the raw data adequately with a minimum adjusted *R*-square value of 0.95. It is clearly evident that in both solvents, the osmotic permeability decreases with increasing membrane rigidity (Fig 7b).

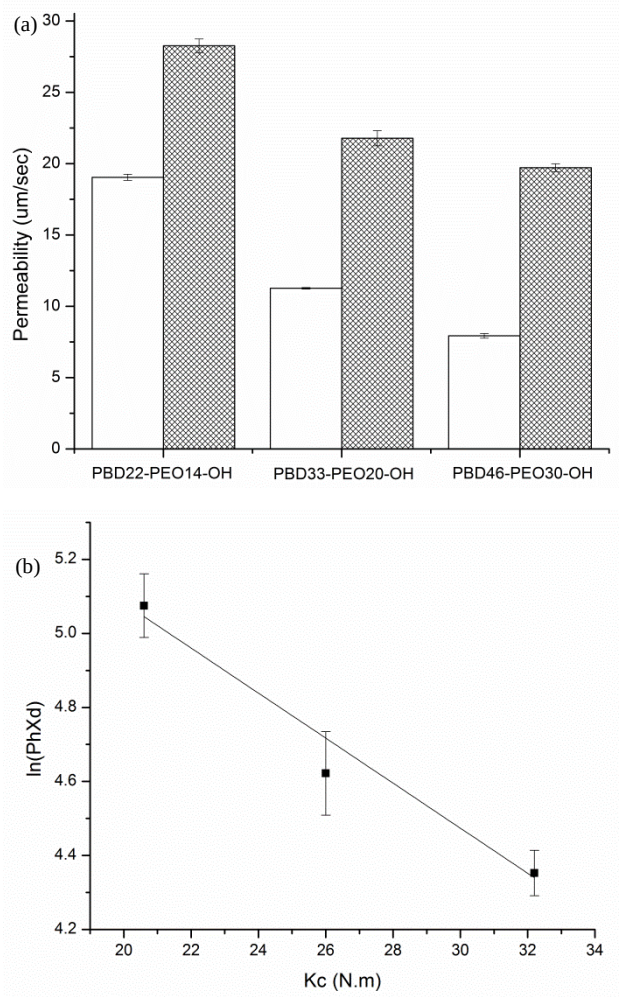

Fig 7. (a) The osmotic permeability (μm/sec) of block copolymersomes in DI water (blank columns) and 1xPBS (filled columns); (b) the graph of ln(P_h×d) versus bending rigidity (κ_c). A strong linearity (adjusted *R*-square = 0.968) indicates that the water permeation rate is dominated by (1) mass transfer at interfacial region; (2) diffusion of solute across the hydrophobic segment in the bilayer.

This correlates well with the hypothesized water permeation mechanism in the block copolymer bilayer that the osmotic permeability is related to the reversible work done required to incorporate solute into the bilayer. The two rate-limiting steps involved are (i) transport of solutes at the interfacial region between the amphiphilic bilayer and the surrounding aqueous solution; and (ii) diffusion across the hydrophobic segment in the bilayer. Equation (3) summarizes the osmotic permeability across the block copolymer bilayer, whereby P_h is osmotic permeability, l is the width of hydrophilic segment, D_{sm} is diffusion coefficient across the interface, d is the thickness of hydrophobic core, D is the diffusion coefficient of solute in the hydrophobic segment, and K' is the mean partition coefficient of water into the hydrophobic segment.[40]

$$\frac{1}{P_h} = \frac{2l}{D_{sm}} + \frac{d}{DK'} \quad (8)$$

$$ln(P_h \times d) \propto \kappa_c \quad (9)$$

A simplification[21] can be made to Equation (8), reducing it to an exponential dependence of the product of osmotic permeability (P_h) and hydrophobic thickness (d) on the bending rigidity of the bilayer (κ_c) (Equation 4). Here, we are able to demonstrate that the osmotic permeability across the block copolymer bilayer, though bearing significant structural dissimilarity to lipid bilayer, is still dependent on the rigidity of the membrane (Fig 7) as a strong linearity exists between these two factors.

An intriguing observation has been made on the permeabilities of the polymersomes dissolved in different solvents, which has not been observed by other research groups, where the ratio of $P_{h(1XPBS)}/P_{h(DI)}$ is proportional to the molecular weight of the polymers. It might merit further studies, and one interpretation of this intriguing result is the possible rearrangement of the hydrophobic core as suggested likewise for the lipid membrane,[41] or a different local hydration of the interfacial region.

3.7 Chemical crosslinking

Additional chemical crosslinking reaction has been conducted to crosslink the adjacent C=C double bonds in the hydrophobic PBD segment via two-step free-radical polymerization. Ammonium persulfate upon dissolving in aqueous solution releases free radicals and thus has been used as the initiator of free radical reaction. The abundance of C=C double bonds on PBD (poly-butadiene) makes it ideal for such free radical addition reaction. For each molecule of diblock copolymer (which contains 20 C=C double bonds), 1 radical initiator was added to initialize the free radical polymerization. Since the reaction generates new free radicals and propagates, this initiator-to-polymer ratio is reasonable enough to ensure sufficient completion of reaction within 24 hour. The chemical crosslinking in the PBD segment renders polymer vesicles to be more rigid with a greater extent of entanglement within the PBD chains. Chemically crosslinked polymersomes can resist dissolution by ethanol or chloroform. This has been verified by measuring the size of the polymersomes in excess ethanol solution; uncrosslinked PBD33-PEO20-OH polymersomes can be dissolved in excess ethanol, indicated by the size peak of 1 nm in the DLS (Dynamic Light Scattering) result; in contrast crosslinked PBD33-PEO20-OH polymersomes can resist dissolution by ethanol, indicated by the persistent size peak of 160 nm in the DLS result (Fig 8). This is due to the fact that

instead of being held together by hydrophobic interaction, the PBD chains are chemically crosslinked and strengthened, which cannot be dissolved by ethanol.

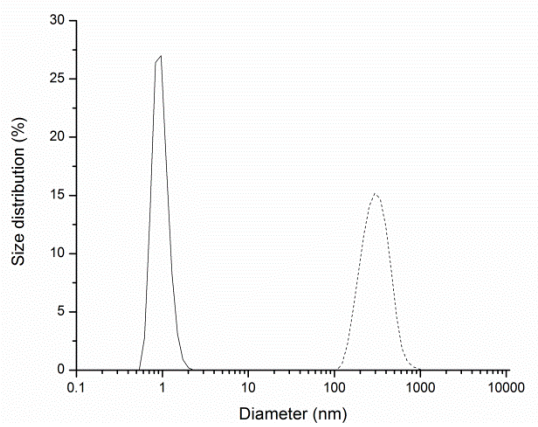

Fig 8. DLS result measures the diameter of the vesicle suspensions: (a) uncrosslinked PBD33-PEO20-OH vesicles (solid line) dissolve in excess ethanol; (b) crosslinked PBD33-PEO20-OH vesicles (dotted line) retain the size even in excess ethanol (~160nm).

It is anticipated that with chemical crosslinking, the polymeric bilayer, in particular the hydrophobic backbone would be rendered more rigid and entangled, accompanied by a decrease in the osmotic permeability. This has been verified by comparing stopped-flow spectroscopy data between the crosslinked and uncrosslinked PBD33-PEO20-OH vesicles. The crosslinked PBD33-PEO20-OH vesicles indeed demonstrate a diminished osmotic flux, however the applicability of the existing formula (Equation 7) for crosslinked vesicles is unclear. Thus the raw stopped flow data has also been included for demonstrating the pronounced effect in the decreased permeability and stretchability of the polymeric bilayer (Fig 9a).

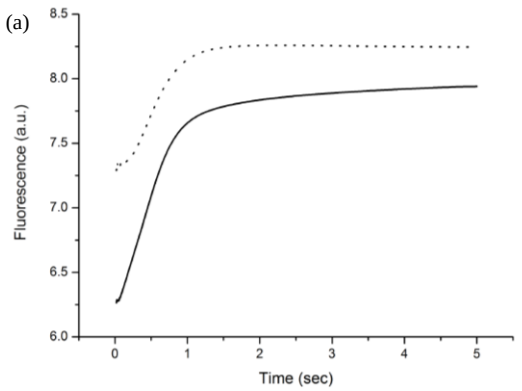

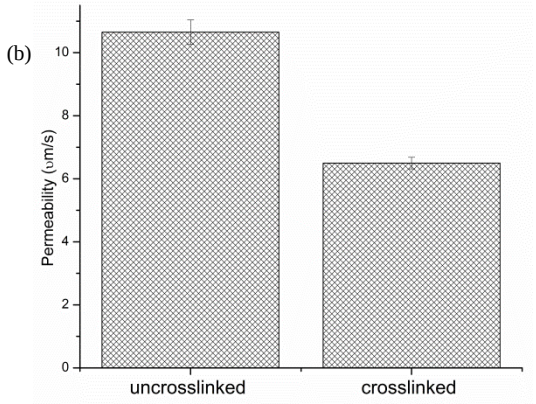

Fig 9. (a) The raw data from stopped flow spectroscopy, showing comparison between crosslinked PBD33-PEO20-OH vesicles (dotted line) and uncrosslinked PBD33-PEO20-OH (solid line); (b) the computed osmotic permeability for both uncrosslinked and crosslinked PBD33-PEO20-OH vesicles.

The osmotic permeability of the pure polymersomes almost halves after chemical crosslinking. As discussed in 3.6 water permeation mechanism, the rate of osmotic permeation through the bilayer is determined by (a) mass transfer at the hydrophobic/hydrophilic interfacial region; (b) diffusion across the hydrophobic segment. Though the diffusion across the hydrophobic segment is already very slow in block copolymer bilayer, chemical crosslinking can effectively decrease the magnitude of diffusion even further, without being absolutely impermeable to osmotic flux. It is hypothesized that the mass transfer and hydration mechanism at the hydrophobic/hydrophilic interfacial region remains fairly consistent before and after the crosslinking, therefore the polymer bilayer is not made completely impermeable to osmotic flux.

4. Conclusions

In this paper, we have studied the mechanistic effects of increasing the molecular weight of block copolymers in modulating the membrane tension and osmotic permeability of polymersomes. The increase in the molecular weight and block length of the block copolymer translates into a direct impact on PEO conformation, bending rigidity modulus (κ_c) and area stretching modulus (κ_a). Our results from LB trough and membrane probe laurdan have confirmed and verified such trend of proportional increase. In addition, we have also examined the osmotic permeability across the polymeric bilayer systematically in a range of different PBD-PEO formulations; more profoundly we are able to demonstrate and establish an interesting relationship between membrane tension (κ_c) and osmotic permeability of an amphiphilic block copolymer bilayer. This mechanistic study reveals that the underlying water permeation mechanism through the amphiphilic block copolymer bilayer involves mass transfer at the interfacial region and diffusion across the hydrophobic segment. With a chemical crosslinking among the neighbouring PBD chains in the hydrophobic segments, the polymeric bilayer could be engineered to be even more rigid to solvent dissolution and less permeable to osmotic flux.

Acknowledgements

This work was financially supported by Singapore's National Research Foundation (NRF) through the Environment and Water Industry Programme Office (EWIPO) EWI projects 0804-IRIS-01 and 1102-IRIS-13-01, NUS grant number R279000293272 and R-706-000-022-279. The authors appreciated the help from Q Lin, S Koh, W Xie, H Wang, B Wang and G Sun for their suggestions help with this work.

Notes and references

[a] *NUS Graduate School for Integrative Sciences and Engineering, 28 Medical Drive, National University of Singapore, Singapore 117456.*
[b] *Department of Chemical and Biomolecular Engineering, National University of Singapore, 4 Engineering Drive 4, 117576, Singapore. Fax: (65) 6779 1936; Tel: (65) 6516 8467; E-mail: chetyw@nus.edu.sg*
[c] *Department of Bioengineering, National University of Singapore, 9 Engineering Drive 1, 117576, Singapore.*
† Electronic Supplementary Information (ESI) available. See DOI: 10.1039/b000000x/

1. V. Malinova, S. Belegrinou, D. D. Ouboter and W. P. Meier, *Adv Polym Sci*, 2010, **224**, 113-165.
2. J. Zimmermann, M. Kwak, A. J. Musser and A. Herrmann, *Methods Mol Biol*, 2011, **751**, 239-266.
3. B. Jeong, Y. H. Bae, D. S. Lee and S. W. Kim, *Nature*, 1997, **388**, 860-862.
4. O. Onaca, D. W. Hughes, V. Balasubramanian, M. Grzelakowski, W. Meier and C. G. Palivan, *Macromol Biosci*, 2010, **10**, 531-538.
5. P. Tanner, P. Baumann, R. Enea, O. Onaca, C. Palivan and W. Meier, *Acc Chem Res*, 2011.
6. S. Y. Yang, J. A. Yang, E. S. Kim, G. Jeon, E. J. Oh, K. Y. Choi, S. K. Hahn and J. K. Kim, *ACS Nano*, 2010, **4**, 3817-3822.
7. Y. Kang, J. J. Walish, T. Gorishnyy and E. L. Thomas, *Nat Mater*, 2007, **6**, 957-960.
8. D. Xiong, Z. Li, L. Zou, Z. He, Y. Liu, Y. An, R. Ma and L. Shi, *J Colloid Interface Sci*, 2010, **341**, 273-279.
9. D. H. Xiong, Z.; An, Y.; Li, Z.; Wang, H.; Chen, X.; Shi, L., *Polymer (Guildf)*, 2008, **49**, 2548-2552.
10. X. Chen, Y. An, D. Zhao, Z. He, Y. Zhang, J. Cheng and L. Shi, *Langmuir*, 2008, **24**, 8198-8204.
11. F. S. Bates and G. H. Fredrickson, *Annu Rev Phys Chem*, 1990, **41**, 525-557.
12. S. Jain and F. S. Bates, *Science*, 2003, **300**, 460-464.
13. G. H. Fredrickson, A. J. Liu and F. S. Bates, *Macromolecules*, 1994, **27**, 2503-2511.
14. Y. Y. Won, A. K. Brannan, H. T. Davis and F. S. Bates, *J Phys Chem B*, 2002, **106**, 3354-3364.
15. A. L. Demirel and H. Schlaad, *Polymer*, 2008, **49**, 3470-3476.
16. J. J. L. M. Cornelissen, M. Fischer, N. A. J. M. Sommerdijk and R. J. M. Nolte, *Science*, 1998, **280**, 1427-1430.
17. M. Ornatska, S. E. Jones, R. R. Naik, M. O. Stone and V. V. Tsukruk, *J Am Chem Soc*, 2003, **125**, 12722-12723.
18. A. Graff, M. Winterhalter and W. Meier, *Langmuir*, 2001, **17**, 919-923.
19. M. Kumar, M. Grzelakowski, J. Zilles, M. Clark and W. Meier, *Proc Natl Acad Sci U S A*, 2007, **104**, 20719-20724.
20. O. S. Andersen and R. E. Koeppe, 2nd, *Annu Rev Biophys Biomol Struct*, 2007, **36**, 107-130.
21. J. C. M. Lee, R. J. Law and D. E. Discher, *Langmuir*, 2001, **17**, 3592-3597.
22. Y. L. Zhang, J. A. Frangos and M. Chachisvilis, *Biochem Biophys Res Commun*, 2006, **347**, 838-841.
23. D. E. Discher and A. Eisenberg, *Science*, 2002, **297**, 967-973.
24. D. E. Discher and F. Ahmed, *Annu Rev Biomed Eng*, 2006, **8**, 323-341.
25. G. Srinivas, D. E. Discher and M. L. Klein, *Nano Lett*, 2005, **5**, 2343-2349.
26. B. M. Discher, Y. Y. Won, D. S. Ege, J. C. M. Lee, F. S. Bates, D. E. Discher and D. A. Hammer, *Science*, 1999, **284**, 1143-1146.
27. G. Srinivas, J. C. Shelley, S. O. Nielsen, D. E. Discher and M. L. Klein, *J Phys Chem B*, 2004, **108**, 8153-8160.
28. J. C. M. Lee, M. Santore, F. S. Bates and D. E. Discher, *Macromolecules*, 2002, **35**, 323-326.
29. J. N. Israelachvili, *Intermolecular and Surface Forces*, Academic Press, 1992.
30. G. Srinivas, D. E. Discher and M. L. Klein, *Nat Mater*, 2004, **3**, 638-644.
31. T. Parasassi, G. De Stasio, G. Ravagnan, R. M. Rusch and E. Gratton, *Biophys J*, 1991, **60**, 179-189.
32. M. J. Borgnia, D. Kozono, G. Calamita, P. C. Maloney and P. Agre, *J Mol Biol*, 1999, **291**, 1169-1179.
33. R. Rodriguez-Garcia, M. Mell, I. Lopez-Montero, J. Netzel, T. Hellweg and F. Monroy, *Soft Matter*, 2011, **7**, 1532-1542.
34. C. Y. Leung, L. C. Palmer, B. F. Qiao, S. Kewalramani, R. Sknepnek, C. J. Newcomb, M. A. Greenfield, G. Vernizzi, S. I. Stupp, M. J. Bedzyk and M. Olvera de la Cruz, *ACS Nano*, 2012, **6**, 10901-10909.
35. C. Y. Leung, L. C. Palmer, S. Kewalramani, B. Qiao, S. I. Stupp, M. Olvera de la Cruz and M. J. Bedzyk, *Proc Natl Acad Sci U S A*, 2013, **110**, 16309-16314.
36. H. P. Duwe and E. Sackmann, *Physica A*, 1990, **163**, 410-428.
37. E. Evans and D. Needham, *J Phys Chem-Us*, 1987, **91**, 4219-4228.
38. R. L. U. Seifert, *Handbook of Biological Physics*, Elsevier Science B.V. , 1995.
39. M. K. a. W. Helfrich, *Phys. Rev. A*, 1991, **44**, 8356-8360.
40. H. E. Bruno J. Zwolinski, Cecil E. Reese, *The Journal of Phyiscal Chemistry*, 1949, **53**, 1426-1453.
41. B. Qiao and M. Olvera de la Cruz, *Journal of Physical Chemistry Letters*, 2013, **4**, 3233-3237.